International Journal of Mechanical, Industrial and Aerospace Sciences
ISSN: 2517-9950
Vol:10, No:5, 2016

Conceptional Design of a Hyperloop Capsule with Linear Induction Propulsion System

Ahmed E. Hodaib, Samar F. Abdel Fattah

***Abstract*—**High-speed transportation is a growing concern. To develop high-speed rails and to increase high-speed efficiencies, the idea of Hyperloop was introduced. The challenge is to overcome the difficulties of managing friction and air-resistance which become substantial when vehicles approach high speeds. In this paper, we are presenting the methodologies of the capsule design which got a design concept innovation award at SpaceX competition in January, 2016. MATLAB scripts are written for the levitation and propulsion calculations and iterations. Computational Fluid Dynamics (CFD) is used to simulate the air flow around the capsule considering the effect of the axial-flow air compressor and the levitation cushion on the air flow. The design procedures of a single-sided linear induction motor are analyzed in detail and its geometric and magnetic parameters are determined. A structural design is introduced and Finite Element Method (FEM) is used to analyze the stresses in different parts. The configuration and the arrangement of the components are illustrated. Moreover, comments on manufacturing are made.

***Keywords*—**High-speed transportation, Hyperloop, railways transportation, single-sided linear induction motor.

I. Introduction

THE main concept of Hyperloop is sending a capsule at a very high speed, approaching sound speed, in a partially-evacuated tube, using electromagnetic propulsion system.

The capsule is levitated using a high-pressure air cushion. An axial-flow air compressor is placed at the nose of the capsule to make use of the relatively-high air pressure at the front of the capsule, hence decreases the aerodynamic drag. The air coming out of the compressor is injected through nozzles at the bottom of the capsule for levitation. The tricky problem is that we must assure that no shockwaves take place on the surface of the capsule, lest the capsule would act like a syringe. The compressor is driven by an electric motor which gets its power from onboard rechargeable DC batteries.

In order to achieve high speeds, the linear induction motor is the most efficient way to produce frictionless thrust able to overcome the aerodynamic drag. A single-sided linear induction motor is designed and optimized to get the maximum speed and thrust possible with the available power source. The SLIM is designed to be compatible with I-section Aluminum rails. The primary part of the motor is a laminated slotted iron core with coils laid in the slots, the electromagnetic induction of these coils produces eddy currents in the rail conductor. According to Lenz's law, an opposing magnetic field is generated and it repels the primary travelling magnetic field; thus, a thrust force acts on the slotted core which is fixed to the bottom of the capsule resulting in a very high speed.

The propulsion system is supplied by AC power. Power inverters and phase converters transform the DC power of the onboard batteries to high-frequency 3-phase AC power. Solar panels cover the tube to recharge the DC batteries. Standard commercial pumps could easily overcome the air leak and maintain the low pressure needed in the tube. The LIM is clean and its maintenance is easy as it has no moving parts or gears. Integrating these subsystems all together, a Hyperloop capsule is designed [1].

Ahmed Hodaib* and S. Abdel Fattah are with the Department of Aeronautical and Aerospace Engineering, Cairo University, Egypt (*Corresponding Author; Phone: +20 11 516 77886; e-mail: ahmedhodaib@hotmail.com).

II. Capsule Configuration

For stability, the location of the CG of the capsule is optimized by placing the compressor motor at the front while the batteries are placed in the rear part. The rotor of the LIM is placed at the bottom. A structural design is made to be compatible with all of the components of the capsule.

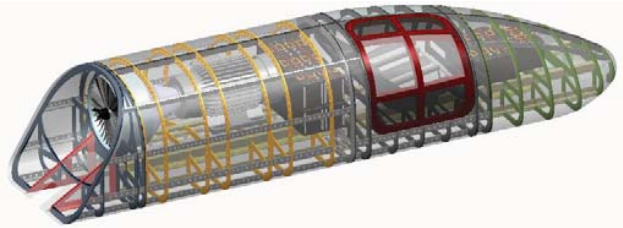

Fig. 1 Configuration of the capsule

III. Aerodynamic Design and Simulation

The design starts with the aerodynamic shape. Generally, the assumption of incompressible flow cannot be made as the vehicle operates at a speed higher than 100 m/s. Hence, the geometry of the tube has a great effect on the air flow. After determining the main requirements such as the dimensions of the capsule and the compressor inlet diameter, an aerodynamic shape can be modelled. Using CFD software, the air flow is solved and the aerodynamic coefficients can be predicted. Besides, reports of velocity, pressure and temperature distributions can be given. After iterating by making modifications and finally getting satisfying results, especially for the drag force which is required to be minimized, we proceed to the next phase of the design [2].

A. Methodology

The governing equations are second order unsteady compressible Navier–Stokes equations in a two-dimensional coordinate system. The flow is simulated as viscous flow and the turbulence model is chosen to be realizable K-ε model. The air inside the tube was assumed ideal gas. The temperature was given initially 288 K [3]. The compressor was assumed to be a mass inlet. The capsule is set as a stationary wall while the tube wall is set as a moving wall with the same velocity of the inlet air. The no-slip condition was applied. The mesh was generated with specific element sizing for certain faces.

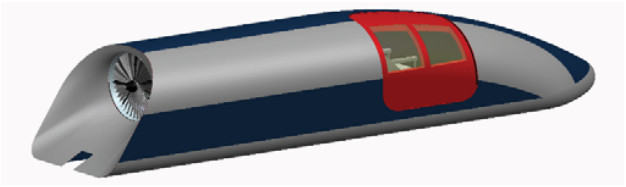

Fig. 2 Aerodynamic shape of the capsule

The main concept is that, if the capsule speed exceeds the critical speed, pressure loss happens due to shockwaves.

After the tube dimensions are determined, the air pressure in the tube is chosen such that it is the minimum pressure sufficient for the compressor, so it results in the minimum drag force without affecting the cushion pressure needed for levitation. The capsule is streamlined to retard the separation of the flow as much as possible, thus decrease the drag force.

B. Results

At a speed of 240 m/s (Mach no.= 0.71), the resulting drag force is 750 N which is a satisfying result. The compressor suction flux is calculated from the levitation requirements to be 2.5 kg/m^2s. The air pressure in the tube is then chosen to be 0.5 KPa. Then, at the air pressure chosen and the operation speed of the capsule, the critical speed is higher than the speed of the capsule. This is verified by the CFD simulations.

Fig. 3 shows the air velocity distribution. The suction made by the compressor results in a low-pressure region in front of the capsule which decreases the drag force.

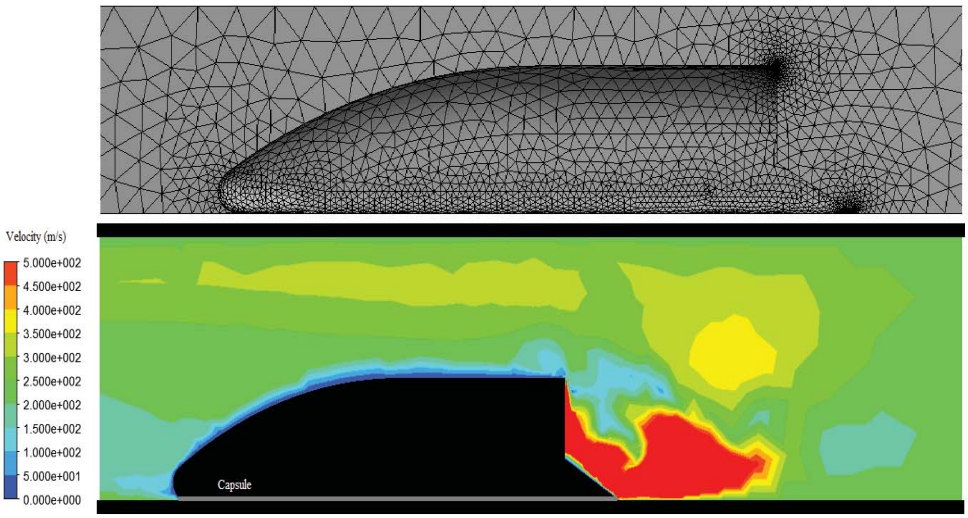

Fig. 3 CFD simulation of the flow around the capsule

IV. Structural Design

The structural design of the capsule was inspired by the aircraft fuselage structure. It consists of transverse frames held apart by longeron channels and stringers. Flanges are used to join the different parts of the structure by bolts. The stressed skin shells are fixed to flanges by rivets. Panel stiffeners are used in some regions in the skin to overcome the bending loads created by the transverse pressure. Local reinforcements are finally integrated in some areas such as the door cut-out. Sharp edging should be avoided as possible to minimize the stress concentration effects [4].

A. Methodology

The design should be based on the worst cases. After understanding the main loads and knowing where to fix each component, the stresses in each part is analyzed using FEM. Each part is meshed then, loads and constraints are applied and its material is chosen. Then, the iterative solver is used to get the equivalent Von-Mises stresses in each element of the analyzed part. Also, reports of the displacements are given.

The structure consists of five parts: The compressor structure, the middle, the seat part, the LIM holding beams and the rear structure.

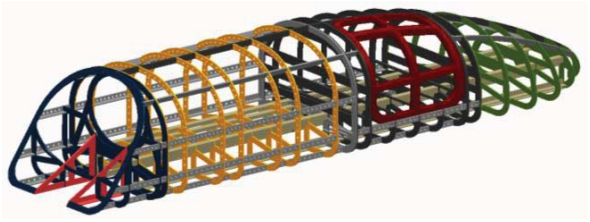

Fig. 4 Structural design of the capsule

The main loads on the pod are determined to be mainly: Axial loads due to thrust acceleration and braking deceleration, Transverse loads due to pressure acting on the skin, Weight distributed loads of the different components, bending moments due to different weight distribution and pressure coefficients on the pod different regions and finally, torsional stresses in the parts holding the compressor. To consider the dynamic loads, the expected static loads are multiplied by a factor.

The main material is chosen to be mainly Steel (Grade 60) for its good thermal properties beside the mechanical properties, and the skin material to be aluminum (Al-7075) for its low surface roughness and high strength-to-weight ratio. The thicknesses of the sheets are changed until it is found that all the results are acceptable for a good margin of safety and all the stresses are within the allowable range. Weight is reduced by reducing the joining areas by the integration of different structure parts. Moreover, the flat pressurized panels and the non-stresses parts are avoided. One other advantage of reducing the joining areas is minimizing the bearing stresses which is difficult to overcome.

B. Sample of the Analysis

Fig. 5 shows the loads acting on the front part of the structure chosen as a sample of the analysis for a specific case as it is one of the complicated parts in the structure, this part is expected to be subjected to loads that are mainly the weight of the compressor acting on the circular frame, a fraction of the weight of the LIM acting on the bottom region and axial loads due to acceleration. Besides, a fraction of load acting on the capsule due to the pressurization. The compressor generates a reaction torque due to its high speed rotation. The constraints are determined where the frame is fixed in the points where the longerons are fastened to them. The 2 bottom longitudinal edges of the LIM area are constrained, as well. A 3D 10-noded tetrahedral mesh is generated where the element size is chosen such that there is minimum of two elements through the part thickness.

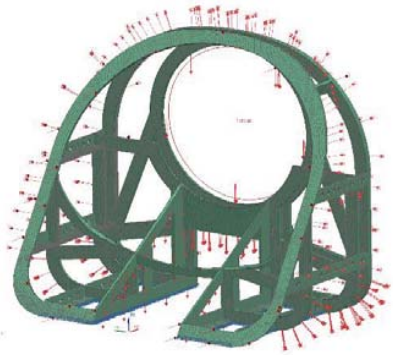

Fig. 5 Meshing the front part and applying the expected loads

The iterative solver creates an idealized part and solves for displacements and stresses using linear statics. The absolute maximum stress is checked and compared to the ultimate tensile stress of the material chosen. The results are satisfying for a certain part if the safety factor is within a good range (2.5 is a reasonable safety factor for this application). Moreover, for weight reduction, modifications are made to the parts that are not stressed.

C. Production

Since most of the structure is made of steel sheets of different thicknesses, it is easy to use laser cutting to cut the required shapes of the different frames from steel strips. Flanges are standard parts, however, some holes are made to be compatible with other parts of the structure. Also most of the longerons are standard section channels. All the parts are assembled using bolts or rivets. The skin shells are riveted to the flanges which is even integrated in the bulkheads or fastened to the frames.

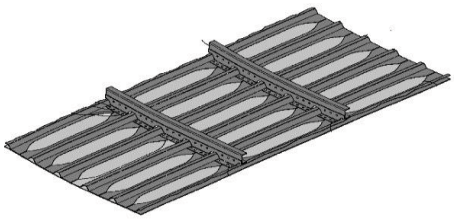

Fig. 6 Stiffened part of the skin

V. Air Bearing Levitation Mechanism

The air cushion performs two functions: to separate the capsule from the tube base, thus eliminating the surface contact and the associated resistance, and to provide the capsule with a suspension system. A Plenum Chamber configuration is used where pressurized air is pumped by a compressor to form the air cushion. Under steady state conditions, the cushion pressure generates a lift force that is equal to the weight of the capsule. The air cushion system gives the capsule sufficient roll and pitch stability. When the capsule rolls, the air gap of the cone on the down-going side is reduced. Consequently, the air flow from that side decreases and the cushion pressure increases. This, together with the decrease of cushion pressure in the cone on the up-going side, provides a restoring moment that tends to bring the capsule back to its original position. A multiple-cone system with a peripheral skirt is designed as shown in Fig. 7. The augmentation factor (K_a) is used to measure the effectiveness of the system and the power required for levitation is determined [5].

A. Methodology

With the assumption that the air in the cushion volume is at rest, and using Bernoulli's theorem to determine the velocity of the escaping air from the cushion gap, an expression for the augmentation factor is derived and is used to design the air cushion system for the capsule. It is proved that the use of a peripheral skirt decreases the amount of the discharging air and increases the effectiveness of the system. Besides, as the hydraulic diameter, which is the ratio between the cushion area and the cushion perimeter, increases, the effectiveness increases and less power is required.

Assuming that there is a pressure ratio (K_p) between the cushion between the skirt and the cones, and the cushion under the cones, the cushion pressure (P_{cu}) can be calculated from (1):

$$F_{cu} = W = P_{cu}A_{c1} + K_pP_{cu}A_{c2} \quad (1)$$

where F_{cu} is the lifting force, W is the weight of the capsule, A_{c1} is the total effective cushion area of the cones and A_{c2} is the effective area between the skirt and the cones.

From Bernoulli's theorem, the velocity of the escaping air under the skirt (V_{c2}) can be computed from (2):

$$V_{c2} = \sqrt{2K_pP_{cu}/\rho} \quad (2)$$

where ρ is the density of air.

The volume flow rate of the escaping air under the skirt (Q_2) can be calculated from (3), and assuming the flow is incompressible, then the volume flow rate from the cones (Q_1) is equal to the volume flow rate under the skirt (Q_2).

$$Q_2 = h_{c2}L_{c2}D_{c2}V_{c2} \quad (3)$$

$$Q_1 = n_ch_{c1}L_{c1}D_{c1}[2(1-K_p)P_{cu}/\rho] = Q_2 \quad (4)$$

where h_{c1} is the clearance height of the cones, L_{c1} is the perimeter of one cone, h_{c2} is the clearance height of the skirt, l_{c2} is the perimeter of the skirt, D_{c1} is the discharge coefficient of the cone, D_{c2} is the discharge coefficient of the skirt and n_c is the number of cones.

From (3) and (4), an expression for the pressure ratio (K_p) can be got.

$$K_p = n_c^2h_{c1}^2L_{c1}^2D_{c1}^2/(n_c^2h_{c1}^2L_{c1}^2D_{c1}^2 + h_{c2}^2L_{c2}^2D_{c2}^2) \quad (5)$$

If we assume a cone diameter (D_{cone}), then the total effective cushion area of the cones (A_{c1}) and the perimeter of one cone (L_{c1}) can be calculated from (6) and (7). A_{c2} can be calculated by subtracting A_{c1} from the total effective cushion area (A_c).

$$L_{c1} = \pi D_{cone} \quad (6)$$

$$A_{c1} = n_c(\pi/4)D_{cone}^2 \quad (7)$$

$$A_{c2} = A_c - A_{c1} \quad (8)$$

The augmentation factor (K_a) is used to measure the effectiveness of the system and the power required (P_a) can be predicted.

$$K_a = (A_{c1} + K_pD_{c1})/(2K_ph_{c2}L_{c2}D_{c2}) \quad (9)$$

$$P_a = P_{cu}Q \quad (10)$$

It can be proven that increasing the effective cushion areas and decreasing the cushion perimeters result in an increase in the augmentation factor. Moreover, decreasing the discharge coefficients results in minimizing the input power required. The discharge coefficient is function of the angle of the wall (or the skirt). For a vertical wall (i.e. with angle 90 degrees), the discharge coefficient is 0.6 approximately.

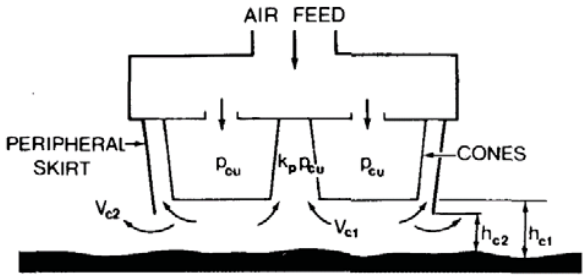

Fig. 7 Multiple-cone air bearing with a peripheral skirt

B. Results

By changing the dimensions of the capsule and the cones number and dimensions, the pressure ratio is calculated. Then, the cushion pressure can be calculated so that it generates a lifting force equal to the capsule weight. The efficiencies of the compressor and its motor are considered, thus this theoretical results have to be corrected using factors. These factors are determined experimentally and they depend on many parameters. On the other hand, we can predict the losses due to friction in the ducts and the cones. After knowing the cushion pressure needed, a multi-stage axial compressor can easily be selected or designed depending on the air pressure in the tube, while an electric motor can be selected to supply the compressor with the required power. Using MATLAB for the design iterations, the following results finally are satisfying.

- Weight $W = 1.5$ tons
- Total effective cushion area $A_c = 2$ m^2
- Perimeter of the skirt $L_{c2} = 9$ m
- Diameter of cone $D_{cone} = 10$ cm
- Number of cones $n_c = 90$
- Clearance heights $h_{c1} = h_{c2} = 2$ cm
- Cushion pressure $P_{cu} = 7.82$ KPa
- Power required $P_a = 440$ HP
- Augmentation factor $K_a = 6.38$

VI. Linear Induction Motor Design

A. Background

Like rotary synchronous motors, linear motors run on 3-phase power and can support very high speeds. However, there are end effects that reduce the motor's thrust force. Linear induction motors are thus less energy efficient than normal rotary motors for any required force output. These end effects include losses in performance and efficiency that are believed to be caused by magnetic energy being carried away and lost at the end of the primary by the relative movement of the primary and secondary. One other parameter that affects the efficiency of the motor and increases the power loss is the air gap between the rotor and the stator of the LIM.

A linear induction motor consists of two parts: The primary part consists of a laminated iron core "thin insulated sheets" with transverse slots that are often straight cut with coils into the slots, with each phase giving an alternating polarity so that

the different phases physically overlap. The secondary part is frequently a sheet of aluminum. Some LIMs are double-sided with one primary on each side of the secondary and some are single-sided.

The thrust force is produced by a linearly moving magnetic field acting on conductors in the field. This conductor that is placed in the field will have eddy currents induced in it thus creating an opposing magnetic field in accordance with Lenz's law. The two opposing fields will repel each other, creating motion as the magnetic field sweeps through the metal.

A linear induction motor may be a short primary, where the primary part is the moving part "the rotor" and the secondary part is the stator, also it may be a short secondary, where the conductive plate is truncated smaller. Generally, the secondary is made wider than the primary to make maximum use of the primary magnetic field.

The motor is short primary, to be compatible with the test track. We found that using a single-sided LIM will minimize the end-effects and also the air gap, as we can put the primary part right over the aluminum I-channel of the rail.

Slipping is the relative motion between the traveling magnetic field and the stator. It is needed to induce voltage in the conductor. A slipping rate of 10% is suitable and a 1-cm air gap is reasonable. However, the motor works properly in a wide range of slipping rate and air gap around these values, but with a slight decrease in the efficiency [6] - [7].

B. Design Steps and Equations

The calculations and iterations are done using a MATLAB script, however they are explained step-by-step. But first, the current sheet concept should be introduced. To study the MMF produced by the coils, we assume a thin layer of current that produces the same sine wave MMF in the air gap as the coils. The equivalent circuit is studied considering the effect of the air gap and the end-effects. Expressions for the values of the equivalent circuit components can be easily derived.

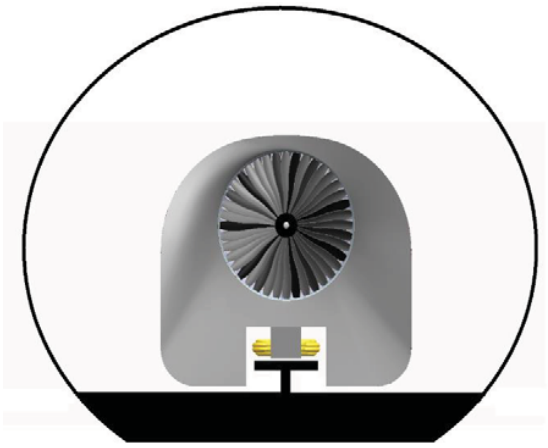

Fig. 8 Front view showing the capsule with the tube cross-section

The design calculations are done in the following sequence [8]:

1) Assigning the constant values to permeability of air (μ_0), the volume resistivity of aluminum (ρ_r), the volume resistivity of copper (ρ_w), the rotor current density (J_1), the maximum tooth flux density (B_{tmax}) and the maximum yoke flux density (B_{ymax}).
2) Specifying desired values for the number of phases (m), the number of slots per pole per phase (q_1), the number of poles (p), the slipping percentage (S), the core width (W_s), the mechanical air gap (g_m), the rail conductor thickness (d), the line voltage (V_{line}), the source frequency (f), the desired rotor velocity (V_r) and the desired thrust force (F_s).
3) The synchronous velocity (V_s) can be calculated from V_r and S.

$$V_s = V_r / (1 - S) \tag{11}$$

4) The RMS voltage (V_1) is computed from V_{line}.

$$V_1 = V_{line} / \sqrt{3} \tag{12}$$

5) The pole pitch (τ), the slot pitch (λ) and the core length (L_s) are calculated.

$$\tau = V_s / 2f \tag{13}$$

$$\lambda = \tau / mq_1 \tag{14}$$

$$L_s = p\tau \tag{15}$$

6) Assuming the slot width and the tooth width are equal $w_s = w_t = \lambda/2$ and putting the number of turns per slot $N_c = 1$.
7) The number of turns per phase (N_1) is computed.

$$N_1 = p\, q_1\, N_c \tag{16}$$

8) Initially guessing a value for $\eta\cos\varphi$ where $0 < \eta\cos\varphi < 1$.
9) The RMS Input Phase Current (I_1) is calculated.

$$I_1 = F_s V_r / (m V_1 \eta\cos\varphi) \tag{17}$$

10) The area of wire for one turn per slot (A_w), slot area (A_s) and the slot height (h_s) are assumed, with the assumption that 30% of the area of the slot is filled with insulation material, and J_1 is the rotor current density.

$$A_w = I_1 / J_1 \tag{18}$$

$$A_s = (10/7)\, N_c A_w \tag{19}$$

$$h_s = A_s / w_s \tag{20}$$

11) The magnetic air-gap (g_0), Carters coefficient (k_c), Equivalent air gap (g_e), the winding factor (k_w) and the goodness factor (G) are calculated.

$$g_0 = g_m + d \tag{21}$$

$$\gamma = (4/\pi)[(w_s/2g_0)\tan^{-1}(w_s/2g_0) - \log_{10}\sqrt{1+(w_s/2g_0)^2}\,] \tag{22}$$

$$k_c = \lambda / (\lambda - \gamma g_0) \tag{23}$$

$$g_e = k_c g_0 \tag{24}$$

$$k_w = \sin(\pi/2m) / [q_1 \sin(\pi/2mq_1)] \tag{25}$$

$$G = 2\mu_0 f \tau^2 / [\pi(\rho_r/d)g_e] \tag{26}$$

12) Per-phase equivalent circuit parameters: the per-phase rotor-slot leakage reactance (X_1), the per-phase rotor winding resistance (R_1), the per-phase magnetizing reactance (X_m) and the per-phase stator resistance (R_2) are calculated from the following expressions which can be easily derived [9].

$$R1 = 2\rho_w(\pi+\tau)J_1N_1 / I_1 \tag{27}$$

$$X_1 = 8\mu_0\pi f (a\pi/q_1 + 0.6\tau) N_1^2 / p \tag{28}$$

$$X_m = 24\,\mu_0\pi f k_w N_1^2 \tau(\pi + g_e) / \pi^2 p g_e \tag{29}$$

$$R_2 = X_m / G \tag{30}$$

where

$$a = (h_s/3w_s)(1+3/p) + 5(g_e/w_s)/(5+4g_0/w_s) \tag{31}$$

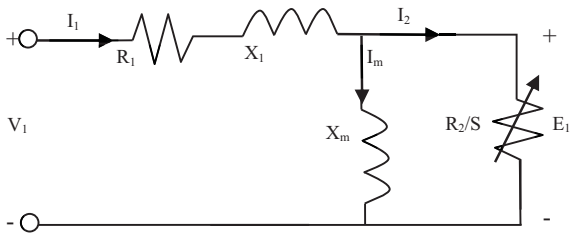

Fig. 9 Schematic showing the components of the equivalent circuit

13) The impedance (Z), the phase angle (φ), cosφ and the magnetizing current (I_m) are calculated.

$$Z = R_1 + j\,[X_1 + (R_2/S)X_m / (R_2/S + jX_m)] \tag{32}$$

$$I_1 = V_1 / |Z| \tag{33}$$

$$I_2 = j\,I_1X_m / (R_2/S + jX_m) \tag{34}$$

$$I_m = I_1 - I_2 \tag{35}$$

where

$$j = \sqrt{-1}$$

14) The power factor (PF) can be calculated from the impedance.

$$PF = \cos\angle(Z) \tag{36}$$

15) At the desired rotor velocity (V_r), we can calculate the actual thrust force (F_s), output power (P_o), input power (P_i) and the efficiency (η).

$$F_s = m|I_1|^2 R_2 / [(1/(S^2G^2)+1)V_sS] \tag{37}$$

$$P_o = F_sV_r \tag{38}$$

$$P_i = P_o + m|I_2|^2 R_2 + m|I_1|^2 R_1 \tag{39}$$

$$\eta = P_o / P_i \tag{40}$$

16) The value of ηcosφ is calculated.

$$\eta\cos\varphi = \eta\,PF \tag{41}$$

17) If the calculated ηcosφ error from the assumed value is less than 1% then proceed to the next step. If not, we repeat from step (9) with a new value of cosφ as in (42).

$$\eta\cos\varphi_{(new)} = (\eta\cos\varphi_{(calculated)} + \eta\cos\varphi_{(old)}) / 2 \tag{42}$$

18) Then checking if the calculated thrust force equals the target thrust force. If not, we increase N_c by 1 and repeat from step (7).
19) Putting the number of parallel wires (N_p) =1.
20) Choosing copper wire diameter (D_w) from standard gauges.
21) Calculating the new values of the slot width (w_s), tooth width (w_t) and the area of wire for one turn per slot (A_w), then calculating the slot height (h_s) from (19) and (20).

$$w_s = D_wN_p \tag{43}$$

$$w_t = \lambda - w_s \tag{44}$$

$$A_w = (\pi/4) N_p D_w^2 \tag{45}$$

22) The magnetic air gap (g_0), Carters coefficient (k_c), the equivalent air gap (g_e) and the goodness factor (G) are calculated again from (21)-(26).
23) Per-phase equivalent circuit parameters: the per-phase rotor-slot leakage reactance (X_1), the per-phase rotor winding resistance (R_1), the per-phase magnetizing

reactance (X_m) and the per-phase stator resistance (R_2) are calculated from (27)-(31).

24) The minimum tooth width (w_{tmin}) is calculated and we check if the tooth width (w_t) is greater than (w_{tmin}). If not, we increment N_p and repeat from step (20).

$$w_{tmin} = 2\sqrt{2}\, m\, k_w N_1 |I_m| \mu_0 \lambda / (\pi\, p\, g_e b_{tmax}) \quad (46)$$

25) Calculating the new RMS Input Phase Current (I_1) again from (17), the actual current density (J_1) can be calculated from (18).

26) Calculating the minimum yoke height (h_y).

$$h_y = 4\sqrt{2}\, m\, k_w N_1 |I_m| \mu_0 L_s / (\pi^2 p^2 g_e b_{ymax}) \quad (47)$$

27) At rated V_r, we can calculate F_s, P_o, P_i and η again from (37)-(40). Finally, we check if the actual thrust force calculated equals the target thrust force. If not, we choose a new wire gauge and repeat from step (21).

C. Winding Configuration

The winding configuration is very important in the design of linear induction motor. The designed motor is with a double-layer-winding full-pitch configuration. "Double-winding" means that each slot contains two coil sides while "Full-pitch" means that the coil span is 180 degrees "one pole pitch". Fig. 10 shows the 3 phases windings in the slots, where the green colored slots are the current input slots (positive) while the red colored slots are the current output (negative).

- Coil span $\theta_p = 180^\circ$ (Full-pitch)
- Double-layer winding
- Number of poles $p = 10$
- Number of slots $N_{slots} = 30$
- Number of phases $m = 3$ (A, B and C)

Fig. 10 Double-winding configuration for the slotted core

D. Results

For a rated velocity of 240 m/s and a thrust force needed to overcome the aerodynamic drag which is equal to 750 N, the geometric and magnetic parameters of the LIM can be determined for the highest possible efficiency with the available power sources.

- Rotor Velocity $V_r = 240$ m/s
- Target Thrust Force $F_s = 790$ N
- Slip Percentage $S = 10\%$
- Frequency $f = 500$ HZ
- Line Voltage $V_{line} = 480$ V
- Aluminum Sheet thickness $d = 1$ cm
- Air gap $g_m = 1$ cm
- Width of core $W_s = 20$ cm

After running the previous calculations on MATLAB using "for" loops for iterations, the final results are:

- Wire diameter $D_w = 5.189$ mm
- Number of turns per coil $N_1 = 1$
- Parallel wires per winding $N_p = 22$
- Length of core $L_s = 2.6667$ m
- Slot width $w_s = 7.4006$ cm
- Tooth width $w_t = 1.4883$ cm
- Minimum tooth width $w_{tmin} = 0.0249$ cm
- Minimum Yoke height $h_{ymin} = 0.0586$ cm
- Minimum Slot height $h_{smin} = 0.3553$ cm
- Slot pitch $\lambda = 8.8889$ cm
- Rated Current Intensity $I_1 = 1.3051e3$ A
- Current density $J_1 = 7.0902e6$ A/m^2
- Actual Thrust Force $F_s = 788.4844$ N
- Input Power $P_i = 282.2895$ HP
- Efficiency $\eta = 0.8998$

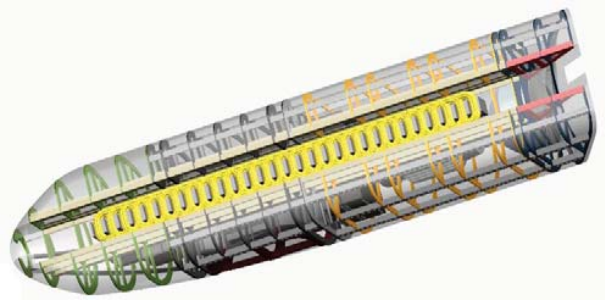

Fig. 11 The rotor fixed to the bottom of the capsule

E. Weight Estimation

To estimate the weight of the rotor of the linear induction motor core. We can, mainly, consider the iron core and the copper wire.

$$W_{wire} = 2\, \rho_{cu}\, A_w\, N_{turns}\, N_{slots}\, (\lambda + W_s) \quad (48)$$

$$W_{core} = \rho_{iron}\, W_s\, (h_y L_s + h_t w_t N_{slots}) \quad (49)$$

$$W_{total} = W_{wire} + W_{core} \quad (50)$$

Then, the estimated total weight of the linear induction motor rotor is 207 kg.

F. Manufacturing

The manufacturing of the linear induction motor rotor is very easy, as there is no moving complicated parts. The core is made of steel laminated, insulated using resin, and put together to form the laminated core. This can be made by using CNC laser cutting or water jet cutting. The core side is drawn on a CAD software and exported as a 2D drawing to be ready for cutting. The copper coil turns are also insulated from each other using resin. Some threaded holes are made in specific parts of the core to be fastened to the structure of the capsule using bolts. Fig. 12 shows a manufactured rotor product [10].

Fig. 12 The core of a linear induction motor product

VII. Navigation System

The inertial navigation system "INS" is completely self-contained and very accurate in measurement. It uses an inertial measurement unit "IMU" (gyroscopes and accelerometers) to maintain an estimate of the position, velocity, and attitude rates of the capsule, and a Computer to run navigation equations. The IMU is sufficient to navigate relative to inertial space, given initial values of velocity, position and attitude by integrating the sensed acceleration, it gives velocity, and a second integration gives position. The integration depends on the attitude, so the sensed angular velocity is integrated. Due to errors in the gyros and accelerometers, an INS will have unlimited drift in velocity, position and attitude. To limit the drift, the INS is usually aided by other sensors that provide direct measurements of, for example, position and velocity. The global positioning system GPS can be used to calibrate the measurements by the means of Kalman filter [11].

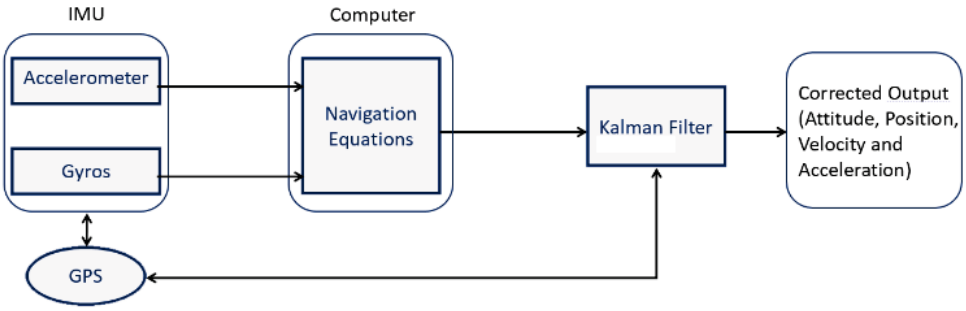

Fig. 13 GPS-aided inertial navigation system chart

Acknowledgment

The authors would like to acknowledge the support of Cairo University and show their sincere appreciation to the great help that were specially provided by the faculty dean, Prof. Sherif Mourad.

References

[1] SpaceX Hyperloop Alpha, Elon Musk.
[2] Harman, Charles M., Davidson, James V., 1977. The drag on vehicle in tunnels. High-Speed Ground Transportation Journal 11 (2), 177–187.
[3] Aerodynamic characteristics of a tube train, Tae-Kyung Kim, Kyu-HongKim, Hyeok-BinKwon, Journal of Wind Engineering and Industrial Aerodynamics, 2011.
[4] Airframe Structural Design, Michael Chun Yung Niu, 1989.
[5] Theory of Ground Vehicles, 4th Edition - J. Y. Wong, 2001, Chapter 8.
[6] Nasar, S.A. and Boldea, I., Linear Electric Motors, Prentice-Hall, Inc., Englewood Cliffs, New Jersey, 1987.
[7] The Induction Machines design handbook; Boldea, Nasar; 2nd Ed., 2010, Chapter 20.
[8] Design of a single-sided linear induction motor (SLIM), by Sarveswara Prasad Bhamidi, May 2005.
[9] A complete equivalent circuit of a linear induction motor with sheet secondary Pai, R.M.; Boldea, I.; Nasar, S.A.; Magnetics, IEEE Transactions on , Volume: 24 , Issue: 1 , Jan. 1988 Pages:639 – 654.
[10] Retrieved: "Linear Induction Motor" from H2W Technologies http://www.h2wtech.com/product/linear-induction/LMB-06-055.
[11] http://www.navlab.net/Publications/Introduction_to_Inertial_Navigation.pdf.

Ahmed E. Hodaib is a 22-year-old bachelor student at the department of Aeronautical and Aerospace Engineering in Cairo University. He is interested in Robotics, Aerodynamics, Propulsion and Turbo-machinery. He was responsible for the robotic manipulator design and manufacturing in LMRT team that participated in Mars Society University Rover Challenge in USA. He also worked on other innovative ideas such as introducing airless tyres to space rovers. In 2016, he participated in SpaceX Hyperloop Competition where he was responsible for the propulsion system, aerodynamics and structural design for the capsule which got a design concept innovation award.

Samar F. Abdel Fattah is a second year Aerospace Engineering student, Cairo University. Started research programs since her first year and joined a research project for interstellar mission to reach Alpha Centauri using solar sails technique with the Initiative for Interstellar Studies in Octobre2015. The project lasted for almost a year and got an innovation award for the mission design. Her team got an innovation award from SpaceX for the pod design at SpaceX design weekend, January, 2016. Samar F. Abdel Fattah is still doing her bachelor degree at Cairo University. However, is still iterating on hyperloop technology as future for transportation.